
**STRENGTH
AND PLASTICITY**

A Neutron Diffraction Study of the Effect of Holdings and Heat Treatment on Residual Stresses in a Steel Weld

I. D. Karpov^{a, *}, V. T. Em^a, I. G. Karpov^b, and A. V. Il'in^b

^a *Kurchatov Institute National Research Center, Moscow, 123182 Russia*

^b *Kurchatov Institute National Research Center, Prometey Central Research Institute of Structural Materials,
St. Petersburg, 191015 Russia*

**e-mail: Karpov_ID@nrcki.ru*

Received April 19, 2022; revised June 28, 2022; accepted June 29, 2022

Abstract—Residual stresses in an X-shaped weld of 32-mm-thick steel plates have been studied using neutron diffraction. The effect of pre-holding of weldments and their post-weld heat treatment on the distribution of residual stresses has been studied. The stress distribution is close to symmetric with respect to the centerline of the weld section and clearly asymmetric with respect to the middle of the weld thickness. The maximum tensile (longitudinal) stresses occur in the weld half-thickness, which was welded first. The peak value of longitudinal stresses in a fixed plate is 800 MPa (98% of the yield strength of the weld metal), which is significantly higher than that in a free plate (530 MPa). The zone of maximum compressive (transverse) stresses of –400 MPa in a fixed plate is located in the first half-thickness of the weld, while its second half occurs in the free plate. After heat treatment, the tensile and compressive stresses remained in general tensile and compressive, respectively. The maximum tensile longitudinal stresses were reduced to 270 MPa in the fixed plate and to 220 MPa in the free plate. The maximum compressive transverse stresses in both plates were reduced to –170 MPa.

Keywords: neutron diffraction, residual stresses, steels, weld, heat treatment

DOI: 10.1134/S0031918X22090058

INTRODUCTION

Molten weld metal after solidification in a welding process is cooled from an extremely higher temperature than the base metal. A large difference in the degree of compression of the weld metal and base one during cooling results in the occurrence of high tensile stresses in the weld [1, 2]. In the case of using ferritic steel as the weld metal, another factor affecting the distribution of residual stresses is the volumetric expansion of the weld metal determined the γ – α phase transition, which results in the formation of compressive stresses in the transition zone.

Residual stresses can considerably degrade the fatigue strength and corrosion resistance of a welded joint [3–8]. Therefore, quantitative information about residual stresses, in particular, the magnitude and location of maximum tensile stresses, is essential for reliable estimating the strength and service life of a welded joint. It is also necessary to verify various calculation models. In the case of thick welds, information about the stresses within the weld is required, since a large number of passes and strong constraining conditions lead to a complicated pattern of the stress distribution over the joint thickness.

To reduce the deformations of structures, weldments are often fixed in various ways; in addition, many welds are located on parts already held together. Stiffening ribs are the most common type of holding. Heat treatment is commonly used to reduce residual stresses. Therefore, it is necessary to have reliable quantitative information on the effect of holding and heat treatment on residual stresses.

Owing to the high penetration capability of neutrons in most metals, neutron diffraction (ND) is the only nondestructive method that makes it possible to measure all three components of the stress tensor in massive bulky components (up to 50 mm thickness in steel) [2, 9]. The X-ray method can be used to measure stresses only on the surface or in the near-surface layers (of ~20 μ m in steel). Therefore, the ND method is currently widely used to measure residual stresses in massive welded joints.

The ND method has been recently widely used to study stresses in welded joints of large-thickness plates (≥ 20 mm) with V-grooves [9–15]. These studies have shown that in single-groove V-welds the maximum longitudinal tensile stresses occur in the upper half of the weld near the surface or at a depth that can reach 40% of the plate thickness. Depending on the techno-

Table 1. The chemical composition of steel and electrodes (wt %)

Material	C	Si	Mn	Cr	Ni	Al	V	Cu	Mo	S	P
Steel	0.10	0.17	0.42	0.75	2.80	0.02	0.08	1.15	0.54	0.005	0.012
Electrode	0.07	0.25	0.70	0.89	2.50			0.92	0.51	0.015	0.012

Table 2. The mechanical characteristics of the base and weld metals

Zone of welded joint	Yield strength, MPa	Ultimate strength, MPa	Elongation, %
Base metal	1040	1140	17
Weld metal	820	910	16

logical parameters of welding (weld width, heat input, bead application sequence, etc.), one maximum is formed on the weld centerline near the upper surface or two maxima are located symmetrically with respect to the weld centerline. In the latter case, the maxima may occur within the zone of the weld metal or beyond it. The peak magnitudes of longitudinal tensile stresses are close to the yield strength of the weld metal and in some cases exceed it.

The stress distribution in welds with X-shaped grooves was experimentally studied for the first time in [16] using the block removal and layering (BRL) method. The plates were fixed before welding with welded stiffening ribs, which were retained during the study. It was shown that in an X-shaped weld of 50-mm thick ferritic steel, longitudinal stresses are tensile both in the weld and base metal; their peak value is 740 MPa (~150% of the yield strength of the weld metal) located on the centerline (CL) of the weld section in the middle of the thickness (root) of the weld. The transverse stresses were tensile in that half-thickness of the weld, which was welded first, and compressive in the second half. When moving from the CL, a local maximum in the thickness distribution of both longitudinal and transverse stresses was retained in the middle of the thickness. After heat treatment at 600°C for 2 h, as well as before heat treatment, a maximum of longitudinal stresses was observed in the weld root, the value of which decreased from 740 to 140 MPa.

The stress distribution over the thickness along the CL of a 50-mm steel weld with an X-shaped groove was studied in [17] using the finite element method (FEM). In contrast to [16], a free welded plate was studied. The distributions of the longitudinal and transverse components were very similar. The maximum stresses occurred at a depth of about 10 mm from both surfaces. In contrast to the results obtained by the BRL method [16], a minimum, but not a maximum of longitudinal and transverse stresses occurred in the weld root. Longitudinal stresses were tensile throughout the thickness; however, transverse stresses changed from tensile near the surfaces to compressive near the middle of the thickness.

One can assume that the discrepancy between the results obtained in [16] and [17] is due to the fact that in the first case fixed plates were studied, and in the second case the plates were free. The aim of this work was to study the residual stresses in an X-shaped steel weld using the nondestructive ND method and to study the effect of holding and heat treatment on the distribution of residual stresses.

EXPERIMENTAL

Sample Preparation

As the base metal, we used a 32-mm thick rolled sheet made of ferritic low-carbon alloy structural steel of Russian production, manufactured by controlled thermal-deformation rolling. The chemical composition (Table 1) and mechanical characteristics of the used steel are similar to that as Armstrong® Ultra 960, Optim 960 QC, XABO 960, and correspond to S960QL grade in accordance with the EN ISO 10025-6 standard. Welding was performed using the manual arc method with piece covered consumable electrodes (MMA/111). Ferrite electrodes of Russian production with a nominal diameter of 4.0 mm with a basic type coating were used as the welding material. The chemical composition of electrodes is presented in Table 1. According to the mechanical characteristics of the deposited metal, these electrodes are similar to ESAB OK 75.75 electrodes and correspond to E85 grade (GOST 9467) and to E 79 A–B grade (EN ISO 18275-A standard).

The mechanical properties of materials experimentally determined using a method similar to the EN 10002-1:2001 standard on samples of a circular cross section 6 mm in diameter and with a working part with a length equal to 5 diameters of the sample, are presented in Table 2.

The edges for welding were grooved using a gas-flame technique followed by mechanical abrasive cleaning. Manual butt welding was performed toward the rolling direction along a two-sided symmetric X-shaped groove into the bead arrangement. The number of layers was seven per side and the total number of passes was 20 per side. A massive reinforcement ~6.5-mm high above the plate surface was made on

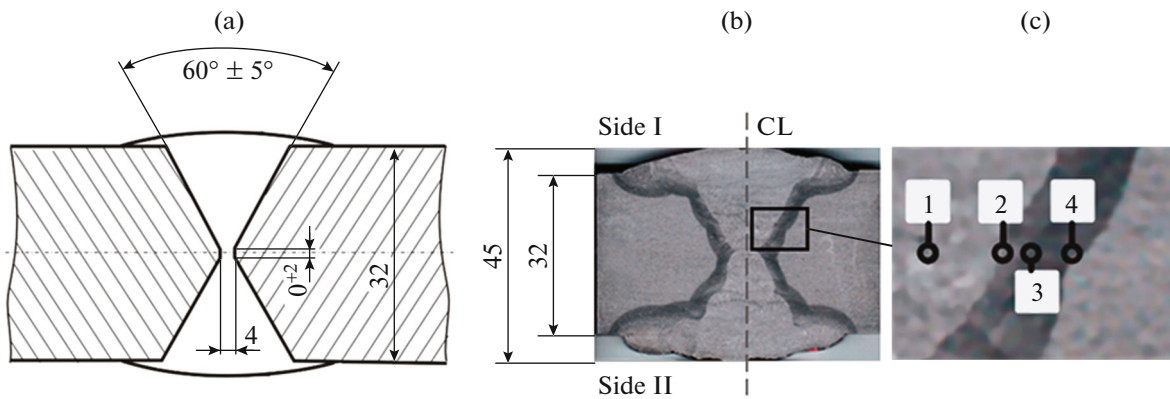


Fig. 1. The X-shaped weld joint: (a) layout of grooves, (b) cross-section of the weld (CL is the centerline of the weld), (c) location of the studied zones of the structure. All dimensions are in millimeters.

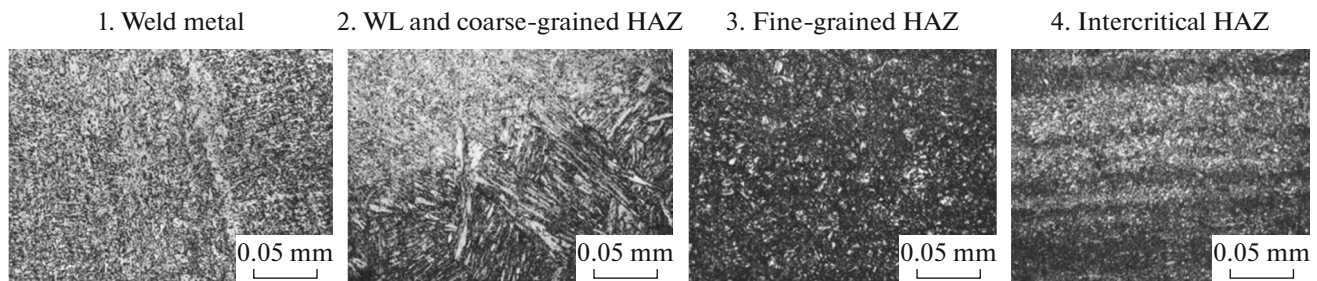


Fig. 2. The microstructure of the weld metal and heat-affected zone (HAZ) shown in Fig. 1c. WL is the weld line.

both sides of the weld in such a way that the weld thickness in the center was ~ 45 mm. The layout of grooves and the metallographic image of the cross-section of the weld are shown in Fig. 1.

Welding was performed with direct current of reverse polarity according to the following regime: current strength 180 A, arc voltage 25 V, welding rate 3.5 mm/s. The estimated input energy was 1.4 kJ/mm. The sheets were preheated before welding to 100°C . The interpass temperature was maintained in the range of $100\text{--}200^{\circ}\text{C}$. At the end of welding, slow cooling was provided using heat-insulating mats.

Figure 2 shows metallographic images of the weld metal and heat-affected zone (HAZ) marked in Fig. 1c. The weld metal exhibits a predominant bainite structure with slightly pronounced ferritic domains. The width of the ferritic bands is $21.5\ \mu\text{m}$. The coarse-grained HAZ exhibits a predominantly martensitic structure. The fine-grained HAZ is identified as bainite with a grain size of $40.7\ \mu\text{m}$. There is no martensite in this zone.

In the intercritical HAZ, increased carbide formation occurred along the boundaries of bainite grains (bainite grain size $32.3\ \mu\text{m}$). The fine-grained and intercritical HAZ exhibits a band structure typical of

the structure of a sheet subjected to thermomechanical processing (namely, rolling). The dimension (thickness) of the HAZ is 3.61 mm.

Four welded joints were prepared in the form of plates with dimensions of 280×400 with a weld located on side 400 (hereinafter, the dimensions are in millimeters). Two samples were fixed before welding with welded stiffening ribs (Fig. 3a); let us denote them as SPs. Two samples were welded in a free state; let us denote them as FPs. The plates were welded on one side (Side I) then turned over and welded on the other side (Side II). The SPs were first welded from the side of stiffening ribs. After welding, the plates of both types were subjected to heat treatment at a temperature of 550°C for 3 h and then cooled in water. Let us denote the plates of two types after heat treatment as HSP and HFP, respectively. Then, parts 100-mm long were cut off using water-jet cutting from the butt end of each welded joint (Fig. 3a) to prepare make a macrosection and d_0 -sample.

Thus, for the studies using the ND method, four samples were prepared in the form of plates $280 \times 300 \times 32$ in size with a weld in the middle (Fig. 3a): two fixed (SP and HSP) and two free (FP and HFP).

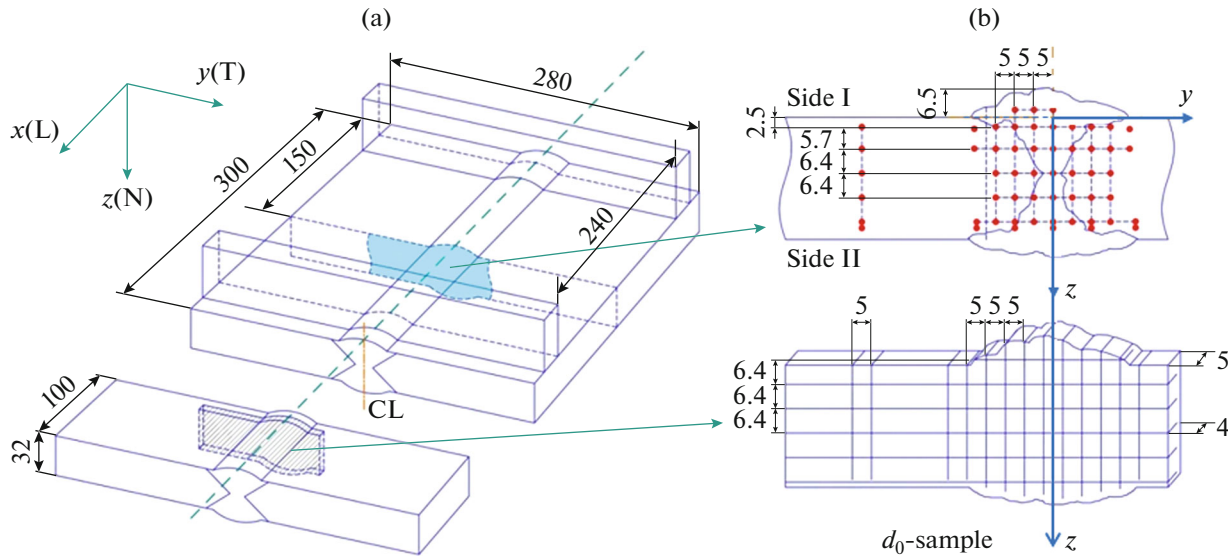


Fig. 3. (a) The layout of the welded plate with stiffening ribs (SP), (b) layout of the points for measurements using the ND method (top) and d_0 -sample (bottom). All dimensions are in millimeters. CL is the centerline of the weld.

Measurement of Stresses Using Neutron Diffraction

The neutron diffraction method of the stress measurements is based on the precise measurement of interplanar space d in the crystal lattice of a material. According to the Wolf–Bragg law $2d\sin\theta = n\lambda$ (n is integer) and interplanar space d can be determined using the neutron diffractometer with constant neutron wavelength λ by precise measuring the diffraction peak with diffraction angle 2θ . The change Δd in the interplanar space results in a $\Delta 2\theta$ shift of the angle of the diffraction peak. The lattice strain ε is determined using the shift of the diffraction peak as follows [2]:

$$\varepsilon = \frac{d - d_0}{d_0} = -(\theta - \theta_0) \cot\theta_0,$$

where d , θ and d_0 , θ_0 are the interplanar space and Bragg diffraction angle in a stressed and stress-free sample, respectively.

The strains along three mutually perpendicular directions (x , y , z) are measured, and the generalized Hook law is used to determine the stresses along these directions [2]:

$$\sigma_i = E[(1 - 2\nu)\varepsilon_i + \nu(\varepsilon_x + \varepsilon_y + \varepsilon_z)] / (1 + \nu)(1 - 2\nu),$$

where $i = x, y, z$; E and ν are the Young’s modulus and Poisson’s ratio, respectively. The stress components in the x , y , and z directions are defined as longitudinal (L), transverse (T) and normal (N) components (Fig. 3). In the experiment, diffraction from a small gauge volume (GV) is measured. This volume is selected in the sample using the cadmium slits placed in the incident and reflected neutron beams. The strain/stress averaged over the GV is measured at each point in the sample.

The residual stresses were studied using a STRESS neutron diffractometer installed at an IR-8 research reactor (the maximum power 8 MW) at the Kurchatov Institute National Research Center using a reactor power of 6 MW. The used original monochromatization scheme makes the possibilities of the device in measuring stresses over depth (50 in steel at GV of 80 mm³ and measurement time of 1 h) comparable with those of other modern facilities at more powerful reactors [18, 19]. A PG(002)/Si(220) double-crystal monochromator made of pyrolytic graphite and bent perfect silicon single crystal produces monochromatic neutrons at a fixed wavelength $\lambda = 0.156$ nm, which is optimum to measure in-depth stresses in ferritic steel [20]. We used the (112) diffraction peak of the bcc lattice of ferritic steel ($2\theta \approx 82^\circ$), which is the least sensitive to microstresses [2]. The GV was set using 3 mm-wide cadmium slits placed in the incident and reflected neutron beams. The slit height in the incident beam was 20 (GV was $3 \times 3 \times 20$) when measuring the normal (z) and transverse (y) components and 5 (CV was $3 \times 3 \times 5$) when measuring the longitudinal (x) component. In both cases, the spatial resolution along the weld thickness was equal to 4. The stress distribution over the depth was measured in the middle of the plate and in the weld cross-section in the points shown in Fig. 3b. We note that $y = 0$ corresponds to the CL, and $z = 0$ corresponds to the plate surface (Side I) at a depth of 6.5 from the weld surface at $y = 0$.

A stress-free sample for measuring d_0 (d_0 -sample) was prepared by electroerosive cutting with wire 0.25 in diameter (Fig. 3). A 5 mm-thick plate was cut from each part 100 mm long cut off from welded joints, and an common “comb” [2] with teeth ($\sim 40(z) \times 5(x) \times 5(y)$) along the normal (z) direction was prepared.

Then, in this comb, to reduce stresses in teeth ~ 40 long [21], several notches (0.25 wide and 4 deep) were made along the transverse (y) direction perpendicular to the teeth. This two-dimensional comb was used as a d_0 -sample.

To calculate the stresses, we used the Young's modulus $E_{112} = 225$ GPa and the Poisson's ratio $\nu_{112} = 0.28$, which correspond to the (112) reflection planes of ferritic steel [2].

RESULTS

Residual Stresses in Samples with Stiffening Ribs

Figure 4 shows the distributions of longitudinal (L) and transverse (T) stresses in SPs and HSPs at distances $y = 0, \pm 5, \pm 10, \pm 15$ from the CL. Figure 5 shows the two-dimensional mappings of the stress distribution in these plates plotted using all measured points.

The distribution of longitudinal and transverse stresses in the SP is close to symmetric with respect to the CL (Figs. 4a, 5a), although the considerable difference in stresses at some symmetric points is observed. The maxima of tensile longitudinal and transverse stresses are located in the weld metal at the depth $z = 2.5$ and $z = 27.5$ (~ 10 from the weld surface) on both sides of the CL ($y = \pm 5$).

The stresses decrease closer to surfaces ($z = -0.25$; $z = 29$) and to the middle of the weld. The highest tensile longitudinal stresses of 800 MPa were observed in the first half-thickness of the weld at Side I ($z = 2.5$, $y = 5$). A local minimum of longitudinal tensile stresses of ~ 270 MPa is observed at a depth of 7.5 along the CL. When moving away from the CL, the local minimum shifts from the first half-thickness to the second one from $z = 7.5$ at $y = 0$ to $z = 20$ at $y = \pm 15$. In this case, the minimum decreases from 270 MPa at $y = 0$ to zero at $y = \pm 10$, and then the transformation into the compressive stresses to -200 MPa at $y = \pm 15$ occurs. The tensile transverse stresses with maxima of 400 MPa are noticeably lower than the longitudinal ones. The compressive transverse stresses are considerably higher than the longitudinal ones, with a maximum of -400 MPa in a wide zone ($-10 \leq y \leq 10$) in the first half-thickness of the weld ($z = 7.5$).

The stresses were considerably reduced after heat treatment (Figs. 4b, 5b). In this case, in general, the tensile and compressive stresses remained tensile and compressive, respectively. The maximum tensile longitudinal stresses were reduced to 270 MPa, and the maximum compressive transverse stresses to -170 MPa.

Residual Stresses in Free Samples

Figure 6 shows the two-dimensional mappings of the stress distribution in FPs and HFPS plotted using the results of the neutron diffraction measurements. Similar to the stress distribution in the SP (Fig. 5a),

the distribution of longitudinal and transverse stresses in the FP (Fig. 6a) is nearly symmetric with respect to the CL and is clearly asymmetric with respect to the middle of the weld thickness.

In general, the distribution of longitudinal stresses is similar to that in the SP; however, they are much lower in magnitude. The peak value (530 MPa) is observed near the surface in the first half-thickness of the weld on Side I ($z = 2.5$, $y = 5$). Similar to the SPs, the tensile transverse stresses are lower than the longitudinal ones.

In contrast to the SP (Fig. 5a), a relatively large zone of compressive transverse stresses with a peak value of -400 MPa is located in the FP in the second half-thickness of the weld, and not in the first one (Fig. 6a).

The stresses were considerably reduced in the HFP after its heat treatment (Fig. 6b). The maximum tensile longitudinal stresses were reduced to 220 MPa, and the maximum compressive transverse stresses were reduced to -170 MPa.

DISCUSSION

An X-groove weld is geometrically symmetric with respect to the center line of the weld section and to the middle of the thickness and can be considered as two V-shaped welds with a root in the middle of the thickness. Therefore, we can expect some similarity and difference in the stress distribution in the X- and V-shaped welds. The distribution of longitudinal and transverse stresses is close to symmetric with respect to the CL (Figs. 5a, 6a), which is consistent with the results of [16] and is typical of V-shaped welds [9–15]. The stress distribution is clearly asymmetric with respect to the middle of the weld thickness, since the first and second half-thickness are welded under different constraining conditions.

In the SP (Fig. 5a), the maximum tensile longitudinal stresses are observed in the weld metal near the surfaces of the plates on both sides of the CL. They gradually decrease by approaching the middle of the weld thickness. The longitudinal stresses are tensile in the entire zone of the weld metal; they decrease with distance from the CL and turn into compressive stresses at a distance of ± 15 from the CL in the base metal of the second half-thickness of the weld. The peak value of longitudinal stresses (800 MPa) in the first half-thickness is close to the yield strength of the weld metal (820 MPa). However, the effective von Mises stress (560 MPa) calculated using the measured values of the longitudinal, transverse and normal stress components, is about 68% of the yield strength. The distributions of longitudinal stresses in the SPs and FPs are similar as a whole (Figs. 5a, 6a). However, the longitudinal stresses in the FP are lower (peak value 530 MPa), and there are no clear maxima on Side II.

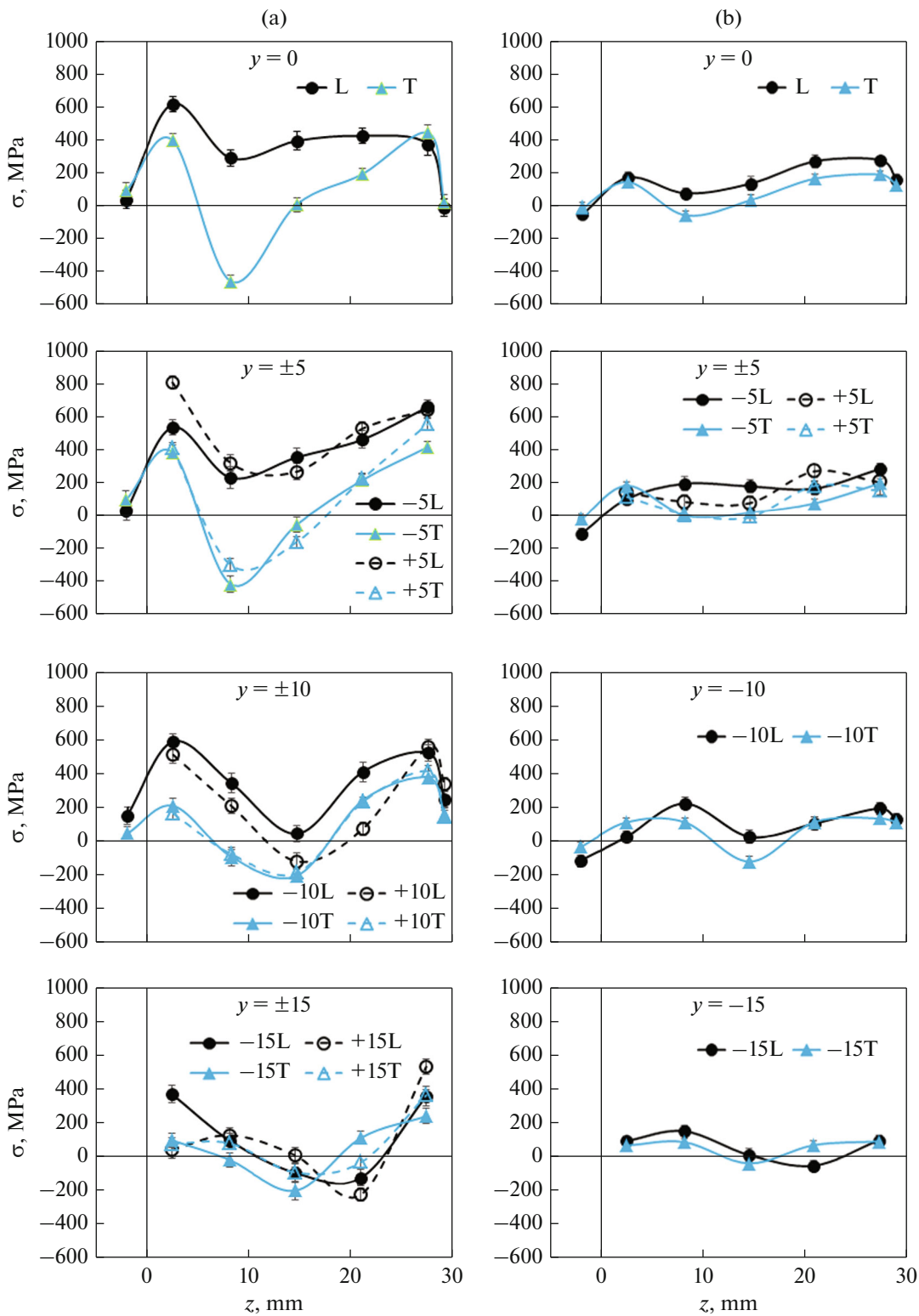


Fig. 4. The distributions of longitudinal (L) and transverse (T) stresses throughout the thickness in (a) SP and (b) HSP at distances $y = 0, \pm 5, \pm 10, \pm 15$ from CL.

The distribution of transverse stresses is clearly asymmetric with respect to the middle of the weld thickness (Figs. 5a, 6a) and depends on the presence

or absence of stiffening ribs. The zone of maximum compressive stresses (-400 MPa) is located in the first half-thickness of the weld in SPs and in the second

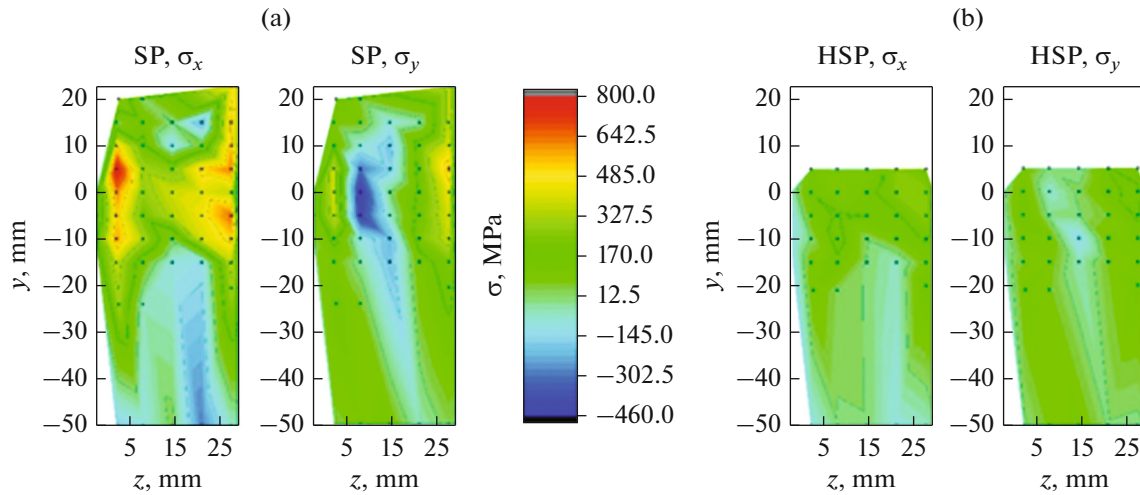


Fig. 5. Two-dimensional mapping of the distribution of longitudinal (σ_x) and transverse (σ_y) stresses in (a) SPs and (b) HSPs.

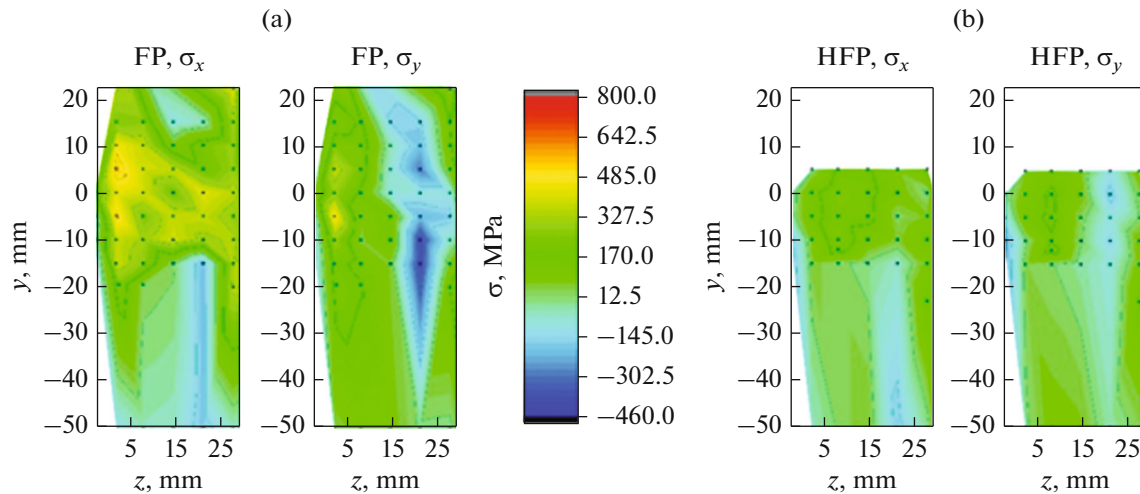


Fig. 6. Two-dimensional mapping of the distribution of longitudinal (σ_x) and transverse (σ_y) stresses in (a) FPs and (b) HFPs.

half-thickness in FPs. In general, in both plates, the tensile longitudinal stresses are higher than the transverse ones, which is consistent with the results of [16]. The higher longitudinal stresses compared to transverse ones are typical of V-shaped welds [13, 22, 23]. The experiments performed in [22] have shown that longitudinal stresses increase with an increase in a weld length. The transverse and normal stresses are much lower and weakly depend on the weld length. This is probably due to the fact that the plate stiffness in the longitudinal direction is higher than in the transverse one.

In contrast to [16], which was performed using the BRL method, in this work, no maxima of longitudinal and transverse stresses were found in the middle of the weld thickness. On the contrary, the stresses decrease near the middle of the weld thickness. The annealing of the previous beads could result in a decrease in stresses in the weld root when depositing next beads [13].

Unexpectedly low stresses ($\sim 10\%$ of the yield strength of the weld metal) were observed in the stiffening near the weld surfaces (Figs. 4, 5a, 6a). In contrast to this, high stresses close to the yield strength were observed on the surface and near the surface of the weld metal [13, 16]. Relatively low stresses ($\sim 30\%$ of the yield strength of the base metal) under the junction points between the weld stiffening and base metal are in poor agreement with the high stresses measured at these points in an X-shaped weld using the BRL method ($\sim 140\%$ of the yield strength of the base metal) [16] and in a V-shaped weld using the ND method ($\sim 100\%$ of the yield strength of the base metal) [13]. The low stresses at these points are probably due to the relatively large sizes of stiffening ribs.

Figure 7 shows the distributions of residual stresses throughout the weld thickness along the CL measured in this work using the DN method and obtained in [16] using the BRL method. To compare the stress dis-

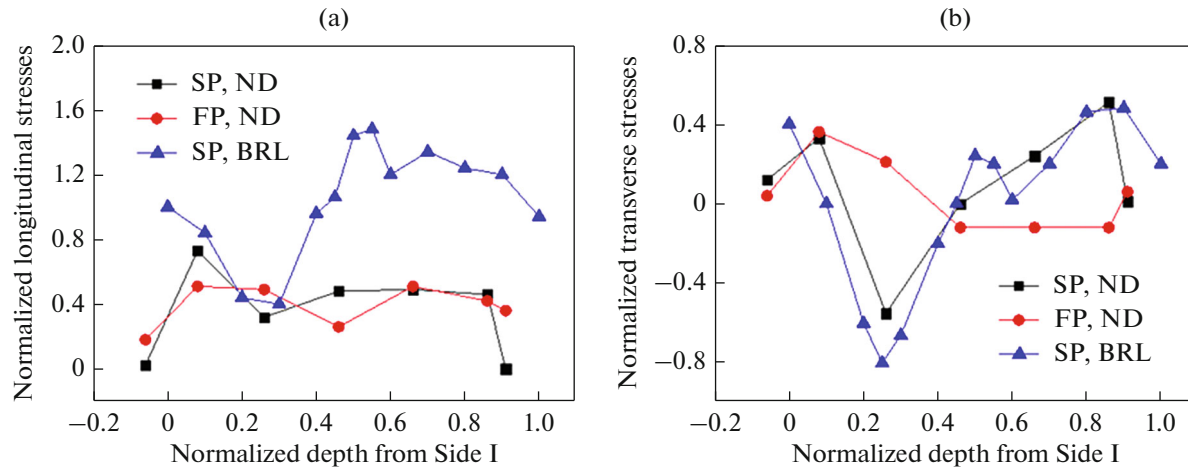


Fig. 7. The distributions of (a) longitudinal and (b) transverse stresses over the weld thickness along the CL in SPs and FPs measured using the ND and BRL [16] methods.

tribution in welds of different thicknesses and of different materials, the depths in plots were normalized by the weld thickness and the stresses were normalized by the yield strength of the corresponding weld metal. There is a strong difference in the distribution of longitudinal stresses obtained using different methods (Fig. 7a). The tensile longitudinal stresses along the CL were revealed using both methods, but the stresses obtained using the BRL method are much higher and at some points exceed the yield strength by 50%. It should be noted that, in addition to differences in the thickness and material of the weld, there are other differences between the samples studied in this work and in [16], which may affect the differences in longitudinal stresses. In samples studied in [16], the yield strength of the base metal was lower than that of the weld metal (360 and 500 MPa, respectively). In our samples, it was the opposite: 1040 and 820 MPa, respectively. The heat input during welding of our samples and those in [16] was also different: ~ 1.4 and $\sim 3 \text{ kJ mm}^{-1}$, respectively. Considering the large discrepancy in the distribution of longitudinal stresses, it was unexpected that there was a large similarity in the distribution of transverse stresses (Fig. 7b); if we do not take into account the local maximum at the weld root obtained in [16]. The transverse stresses are probably less sensitive to welding parameters and more sensitive to the presence or absence of stiffening ribs.

Comparison of the plates before and after heat treatment shows that after heat treatment the stresses are significantly reduced, but the tensile and compressive stresses remain tensile and compressive, respectively.

In contrast to [16], local stress maxima in the middle of the thickness of the weld were not detected in heat-treated samples similar to unannealed samples. The longitudinal stresses remained higher than the transverse ones. In a plate with stiffening ribs, the maximum tensile longitudinal stress (270 MPa, 33%

of the yield strength of the weld metal) is higher than that in a free plate (220 MPa, 28% of the yield strength of the weld metal), which is consistent with the results obtained in [16].

CONCLUSIONS

A nondestructive neutron diffraction method was used for the first time to study the effect of holdings and heat treatment on the distribution of residual stresses in a steel X-shaped weld. The results of the performed studies make it possible to draw the following conclusions:

(1) The stress distribution in the X-shaped weld is close to symmetric with respect to the centerline of the weld section and clearly asymmetric with respect to the middle of the weld thickness.

(2) The distributions of longitudinal tensile stresses in plates with stiffening ribs and in free plates are similar. In both plates, there are two maxima near the surface on Side I in the weld metal on both sides of the centerline of the weld section. In a plate with stiffening ribs, the peak value of longitudinal stresses of 800 MPa (98% of the yield strength of the weld metal) is higher than in a free plate (530 MPa, 65% of the yield strength of the weld metal).

(3) The distribution of transverse stresses strongly depends on the presence or absence of holdings. In a plate with stiffening ribs, the zone of maximum compressive transverse stresses of -400 MPa is located in the first half-thickness of the weld, and in a free plate, it is located in the second half-thickness.

(4) Residual stresses in the stiffening (10% of the yield strength of the weld metal) and under the junction points between the stiffening and base metal (30% of the yield strength of the base metal) are considerably lower than the yield strengths of the corresponding metals.

(5) After heat treatment, the maximum tensile longitudinal and compressive transverse stresses considerably decreased, but remained tensile and compressive, respectively. In a plate with stiffening ribs, the maximum tensile longitudinal stress (270 MPa, 33% of the yield strength of the weld metal) is slightly higher than that in a free plate (220 MPa, 28% of the yield strength of the weld metal). The maximum compressive transverse stresses (−170 MPa) are the same in both plates.

ACKNOWLEDGMENTS

This study was performed using the equipment of the unique Neutron research complex based on an IR-8 reactor scientific facility.

CONFLICT OF INTEREST

The authors declare that they have no conflicts of interest.

REFERENCES

- P. J. Withers and H. K. Bhadeshia, “Residual Stress – II: Nature and Origins,” *Mater. Sci. Technol.* **17**, 366–375 (2001).
- M. T. Hutchings, P. J. Withers, T. M. Holden, and T. Lorentzen, *Introduction to the Characterization of Residual Stress by Neutron Diffraction*, 1st ed. (Taylor and Francis, London, 2005).
- M. Mochizuki, “Control of welding residual stress for ensuring integrity against fatigue and stress–corrosion cracking,” *Nucl. Eng. Des.* **237**, 107–123 (2007).
- N. Winzer, A. Atrens, W. Dietzel, V. S. Raja, G. Song, and K. U. Kainer, “Characterisation of Stress Corrosion Cracking (SCC) of Mg–Al Alloys,” *Mater. Sci. Eng., A* **488** (1–2), 339–351 (2008).
- Z. Barsoum and I. Barsoum, “Residual stress effects on fatigue life of welded structures using LEFM,” *Eng. Fail. Anal.* **16**, 449–467 (2009).
- L. Doremus, J. Cormier, P. Villechaise, G. Henaff, Y. Nadot, and S. Pierret, “Influence of residual stresses on the fatigue crack growth from surface anomalies in a nickel-based superalloy,” *Mater. Sci. Eng., A* **644**, 234–246 (2015).
- X. Cheng, J. W. Fisher, H. J. Prask, T. Gnaupel-Herold, B. T. Yen, and S. Roy, “Residual stress modification by post-weld treatment and its beneficial effect on fatigue strength of welded structures,” *Int. J. Fatigue* **25**, 1259–1269 (2003).
- M. Xu, J. Chen, H. Lu, J. Xu, C. Yu, and X. Wei, “Effects of residual stress and grain boundary character on creep cracking in 2.25Cr–1.6W steel,” *Mater. Sci. Eng., A* **659**, 188–197 (2016).
- W. Woo, V. T. Em, P. Mikula, G. B. An, and B. Seong, “Neutron diffraction measurements of residual stresses in a 50mm thick weld,” *Mater. Sci. Eng., A* **528**, 4120–4124 (2011). <https://doi.org/10.1016/j.msea.2011.02.009>
- A. M. Paradowska, J. W. H. Price, T. R. Finlason, R. B. Rogge, R. L. Donaberger, and R. Ibrahim, “Comparison of neutron diffraction measurements of residual stress of steel butt welds with current fitness-for-purpose assessments,” *J. Pressure Vessels Technol. Trans. ASME* **132**, 051503-7 (2010).
- W. Woo, G. An, E. Kingston, A. Dewald, D. Smith, and M. R. Hill, “Through-thickness distributions of residual stresses in two extreme heat-input thick welds: a neutron diffraction, contour method and deep hole drilling study,” *Acta Mater.* **61**, 3564–3574 (2013).
- D. J. Smith, G. Zheng, P. R. Hurrell, C. M. Gill, B. M. E. Pellereau, K. Ayres, D. Goudar, and E. Kingston, “Measured and predicted residual stresses in thick section electron beam welded steels,” *Int. J. Pressure Vessels Piping* **120–121**, 66–79 (2014).
- H. Alipooramirabad, A. Paradowska, R. Ghomashchi, A. Kotousov, and M. Reid, “Quantification of residual stresses in multi-pass welds using neutron diffraction,” *J. Mater. Process. Technol.* **226**, 40–49 (2015).
- W. Jiang, W. Woo, Y. Wan, Y. Luo, X. Xie, and S. T. Tu, “Evaluation of through-thickness residual stresses by neutron diffraction and finite-element method in thick weld plates,” *J. Pressure Vessel Technol.* **139**, 031401-11 (2017).
- Y. Wan, W. Jiang, J. Lu, G. Sun, D. K. Kim, W. Woo, and S. T. Tu, “Weld residual stresses in a thick plate considering back chipping: neutron diffraction, contour method and finite element simulation study,” *Mater. Sci. Eng., A* **699**, 62–70 (2017).
- D. J. Smith and S. J. Garwood, “Influence of postweld heat treatment on the variation of residual stresses in 50 mm thick welded ferritic steel plates,” *Int. J. Pressure Vessels Piping* **51**, 241–256 (1992).
- Y. Shim, Z. Feng, S. Lee, D. Kim, J. Jaeger, J. C. Parritan, and C. L. Tsai, “Determination of residual stresses in thick-section weldments,” *Weld. Res. Suppl.* **71**, 305–312 (1992).
- V. T. Em, A. M. Balagurov, V. P. Glazkov, I. D. Karpov, P. Mikula, N. F. Miron, V. A. Somenkov, V. V. Sumin, J. Šaroun, and M. N. Shushunov, “A double-crystal monochromator for neutron stress diffractometry,” *Instr. Exp. Technol.* **60**, 526–532 (2017).
- V. T. Em, I. D. Karpov, V. A. Somenkov, V. P. Glazkov, A. M. Balagurov, V. V. Sumin, P. Mikula, and J. Šaroun, “Residual stress instrument with double-crystal monochromator at research reactor IR-8,” *Phys. B: Condens. Matter* **551**, 413–416 (2018). <https://doi.org/10.1016/j.physb.2018.02.042>
- W. Woo, V. T. Em, B. Seong, E. Shin, P. Mikula, J. Joo, and M. Kang, “Effect of wavelength-dependent attenuation on neutron diffraction stress measurements at depth in steels,” *J. Appl. Crystallogr.* **44**, 747–754 (2011). <https://doi.org/10.1107/S0021889811018899>
- S. Ganguly, L. Edwards, and M. E. Fitzpatrick, “Problems in using a comb sample as a stress-free reference for the determination of welding residual stress by diffraction,” *Mater. Sci. Eng., A* **528**, 1226–1232 (2011).
- C. Ohms, P. Hornak, R. Wimpory, and A. G. Youtsos, “Residual stress analyses based on neutron diffraction in double-V butt welded steel plates,” *J. Neutron Res.* **11**, 273–276 (2003).
- H. Suzuki and T. M. Holden, “Neutron diffraction measurements of stress in an austenitic butt weld,” *J. Strain Anal.* **41** (8), 575–581 (2006).

Translated by N. Podymova